Journal of Physics D: Applied Physics

PAPER • OPEN ACCESS

High-sensitive dual-mode thermoreflectance microscopy for the stationary and transient thermal analysis of microelectronic devices

To cite this article: Chan Bae Jeong *et al* 2025 *J. Phys. D: Appl. Phys.* **58** 085101

View the article online for updates and enhancements.

You may also like

- Relationship between the photoionization and fast streamers in Ester-based insulating oil
Kaizheng Wang, Ruilong Yu, Shuaiqi Wang et al.

- Doped--doped transferred electron device for sustained terahertz signal generation
Duu Sheng Ong

- Electron emission characteristics of cathode micro-protrusion and the comparison with the MG theory analysis
Yuanzhao Li, Jiangang Ding, Zhiyuan Liu et al.

UNITED THROUGH SCIENCE & TECHNOLOGY
ECS The Electrochemical Society
Advancing solid state & electrochemical science & technology
248th ECS Meeting
Chicago, IL
October 12-16, 2025
Hilton Chicago
Science + Technology + YOU!
SUBMIT ABSTRACTS by March 28, 2025
SUBMIT NOW

This content was downloaded from IP address 165.194.94.6 on 23/12/2024 at 04:14

OPEN ACCESS
IOP Publishing
Journal of Physics D: Applied Physics
J. Phys. D: Appl. Phys. 58 (2025) 085101 (10pp)
https://doi.org/10.1088/1361-6463/ad9612

High-sensitive dual-mode thermoreflectance microscopy for the stationary and transient thermal analysis of microelectronic devices

Chan Bae Jeong[1,6], **Dong Uk Kim**[1,6], **Ilkyu Han**[1], **Dongmok Kim**[1], **Hwan Hur**[1], **I Jong Kim**[1], **Kye-Sung Lee**[1], **Jung-Dae Kim**[2], **Woo June Choi**[3,4,*] and **Ki Soo Chang**[1,3,5,*]

[1] Division of Scientific Instrumentation, Korea Basic Science Institute, Daejeon 34133, Republic of Korea
[2] Division of Digital Health Research, Korea Institute of Oriental Medicine, Daejeon 34054, Republic of Korea
[3] School of Electrical and Electronics Engineering,Chung-Ang University, Seoul 06974, Republic of Korea
[4] Department of Intelligent Semiconductor Engineering, Chung-Ang University, Seoul 06974, Republic of Korea
[5] School of Bio-Analytical Science, University of Science and Technology, Daejeon 34113, Republic of Korea

E-mail: cecc78@cau.ac.kr and ksc@kbsi.re.kr

Received 13 September 2024, revised 29 October 2024
Accepted for publication 22 November 2024
Published 13 December 2024

Abstract

This study presents a straightforward, efficient dual-mode thermoreflectance microscopy (TRM) system for analyzing the stationary and dynamic thermal properties of microelectronic devices. The proposed TRM system employs a standard visible microscope and implements two distinct imaging process schemes to obtain thermal images at different time scales. For TRM imaging of an ohmic microdevice, the optimal probing wavelength is predetermined from the thermoreflectance spectrum, acquired using a white light-emitting diode source and tunable bandpass filters to enhance thermal sensitivity. Thermoreflectance images are obtained in both stationary and transient modes using a four-bucket method and a pulsed boxcar averaging method, respectively. This thermography approach demonstrates highly sensitive, time-integrated stationary thermal imaging and time-gated transient thermal imaging with a temporal resolution of 200 ns. The system shows significant potential as an analytical tool with a sub-micron spatiotemporal resolution for evaluating heat generation and self-heating behavior in microelectronic devices.

[6] These Authors contributed equally to this work.
[*] Authors to whom any correspondence should be addressed.

Original content from this work may be used under the terms of the Creative Commons Attribution 4.0 licence. Any further distribution of this work must maintain attribution to the author(s) and the title of the work, journal citation and DOI.

© 2024 The Author(s). Published by IOP Publishing Ltd

Supplementary material for this article is available online

Keywords: thermoreflectance imaging, transient thermoreflectance, thermal imaging, transient temperature

1. Introduction

Electronic devices have undergone significant miniaturization, driven by the demand for higher performance and greater integration within integrated circuits (ICs). This trend resulted in an increase in both the density of electronic devices within a single IC and their power consumption. Thus, the thermal behavior of components miniaturized to the sub-microscale exhibits unconventional characteristics in terms of both time and space. The rate of internal heat flux has surged to hundreds of kW cm^{-2}, whereas the thermal response time has drastically shortened to the sub-microsecond range [1–3]. Moreover, the self-heating phenomenon in which a portion of power consumption is transformed into thermal energy can induce localized and rapid temperature rises compared with bulk devices, adversely affecting the performance and lifespan of the microdevice [4–7]. To understand the mechanisms of such self-heating phenomena temporally and spatially, examining both the stable thermal distribution in the sub-micro region and the transient thermal events occurring at or beyond the microsecond level is critical. Consequently, a thermal imaging technique that can analyze both stationary and transient thermal behaviors with high temporal and spatial resolution is essential for enhancing the performance and extending the lifespan of miniaturized electronic devices.

Thermography techniques for semiconductors and microelectronic devices include liquid crystal thermography and fluorescence microthermography, which are semi-invasive thin coating methods; scanning thermal microscopy (SThM), which is based on scanning probe microscopy; and infrared thermography (IRT) and thermoreflectance microscopy (TRM), which are optical techniques [8–11]. These techniques have different spatial and temporal resolutions and should be selected according to application requirements.

SThM is a scanning probe-based thermal imaging method that utilizes a thermocouple at the probe tip. Although SThM is particularly effective for mapping localized temperature distributions at the nanoscale, its contact-based nature could be a limitation, requiring direct interaction with the sample surface [10]. In contrast, non-contact methods such as IRT and TRM are widely used for hot spot detection, failure analysis, and the measurement of temperature distribution and thermal transients, offering efficient thermal management without physically interacting with the sample. IRT, extensively used in the semiconductor industry, detects thermal radiation from 3 to 10 μm in wavelength and visualizes it as a temperature distribution [12]. However, its diffraction-limited spatial resolution is generally restricted to the micron scale because of the wavelength detection range of IR thermal radiation mentioned above. Moreover, achieving temporal resolution at the microsecond scale is challenging because of the infrared thermal camera's frame rate limitations. An alternative thermal imaging technique, TRM, enables the analysis of thermal behavior by detecting relative changes in a sample's reflectivity due to temperature variations [3, 13–15]. Compared with IRT, TRM exhibits superior spatial and temporal resolution [16, 17]. TRM incorporates visible wavelength (0.4–0.7 μm) illumination to measure variations in light intensity reflected from the sample surface to achieve sub-micron spatial resolution [3, 18]. Furthermore, sub-microsecond-scale temporal resolution can be achieved using the pulsed boxcar averaging method, circumventing the limitations imposed by camera frame rates [19, 20].

However, the thermoreflectance coefficient, which represents the degree of reflectivity change with the temperature, is small, typically from 10^{-5} to 10^{-3} K^{-1}. This coefficient considerably depends on the composition of the sample, its layered structure, and the illumination wavelength. Consequently, to achieve an adequate signal-to-noise ratio (SNR) in the measurement of thermal behavior for each sample under test (SUT), selecting an illumination wavelength that corresponds to a high thermoreflectance coefficient is necessary [21–23]. This limitation becomes pronounced when measuring transient thermal phenomena because the lower the temporal resolution is, the smaller the SNR becomes.

The optimal illumination wavelength based on the spectral dependence of the thermoreflectance coefficient can be selected by using two methods. In the conventional TRM approach, the spectral dependence is derived from thermoreflectance images that are repeatedly acquired using light-emitting diodes (LEDs) of different colors or a white light source combined with a linear variable filter [23, 24]. Alternatively, the spectral dependence can be measured in a single acquisition by modifying an optical microscope to provide spectroscopic imaging [21, 25]. However, the first approach yields limited spectral information, whereas the second approach, despite providing extensive spectral information, is challenging to manage because of the complexity of the optical systems involved.

In this study, we report an implementation of a simple and efficient TRM approach to analyze both stationary and dynamic thermal characteristics. First, we proposed a simple configuration of the dual-mode TRM system along with the methods for acquiring thermoreflectance ($\Delta R/R$) images in modes. Subsequently, to validate the system's feasibility, we demonstrated the selection of an optimal illumination wavelength. This selection is based on the thermoreflectance

spectrum obtained by using a white LED light source combined with a filter turret. With the selected illumination wavelength, we captured both stationary and transient thermal images of a microheating resistor.

2. Experimental set-up and sample description

Figure 1 illustrates the schematic of a home-made dual-mode TRM system. The system is based on a user-configurable optical microscope (SFM2, Thorlabs, USA) equipped with an illuminator module including a rotating optical filter turret (CSE2000, Thorlabs, USA), beam splitter (BSW26R, Thorlabs, USA), band pass filter (FBH series, Thorlabs, USA), and objective lens turret (manual turret, Mitutoyo, Japan). An sCMOS camera (PCO.edge 4.2LT, PCO Image, Germany), a white LED light source (MCWHL7, Thorlabs, USA), and an objective lens (50×, NA 0.42, M Plan Apo NIR, Mitutoyo, Japan) were affixed to the microscope assembly for capturing images. The white LED, with a color temperature of 6500 K, illuminated the sample through the objective lens, and the light reflected from the sample was subsequently transmitted back through the objective lens and the filter turret before being captured by the camera. The BPF was positioned within the filter turret that selectively allowed only light of a specific wavelength range from the white LED light source to reach the camera.

The system's operations were controlled through an integrated driver module paired with a LabVIEW based control program. We custom-built the integrated driver module by using a field programmable gate array with an internal reference clock of 100 MHz in order to generate both triggering and synchronizing voltage signals and driving current signals. This module coordinated the voltage signals that govern the functionality (triggering and synchronization) of the camera and bias equipment as well as the current signals that activate the LED light source in either a continuous wave (CW) or a pulsed mode. The integrated driver module provides a voltage signal with transistor-transistor logic (TTL) in the range of 1 Hz–1 kHz and current signal with an output of up to 2 A in a range from DC to 1 kHz. The pulse width and delay of the LED light source can be controlled in the range of 5 ns–499.995 μs. Thermal images within the dual-mode TRM system were captured in both stationary and dynamic states, using the four-bucket method for stationary imaging and the pulsed boxcar averaging method for dynamic imaging, as detailed in sections 3 and 4, which emphasize the system's imaging capabilities in each mode. As illustrated in figure 1 for stationary imaging, the integrated driver module concurrently generated the current signal to power the illumination source in the CW mode and the control voltage signals for the camera and bias equipment, which are necessary for implementing the four-bucket method.

The white LED-light source was powered by a continuous driving current, emitting a steady stream of light. The camera captured reflection (I) images at a frame rate of 4 fps, triggeredby a 4 Hz TTL signal with a 90% duty cycle. The exposure time for each image was set to 225 ms. The bias equipment (SMU2611B, TEKTRONIX, USA) generated a 1 Hz sinusoidal signal that oscillates between 0 and 20 V, triggered by a 1 Hz TTL signal with a 50% duty cycle. Crucially, the maximum bias voltage applied can vary. This bias was applied to the sample to artificially create temperature fluctuations in accordance with the bias voltage. The camera captured I images to detect corresponding changes in reflectivity due to these temperature variations. Using the four-bucket method, stationary $\Delta R/R$ images were subsequently calculated from captured I images. In the transient mode, as depicted in figure 1, the integrated driver module provides the necessary current signal for activating the illumination source in the pulsed mode, along with control voltage signals for the camera and bias equipment tailored for the pulsed boxcar averaging method.

The white LED emitted a series of light pulses, modulated by a driving current that switches on and off at a frequency of 1 kHz. The duration of the pulse width for the driving current varied between 50 ns and 10 μs. An exposure time of 225 ms was used to capture the I images similarly to the stationary mode. The bias equipment (WMA-300, Falco Systems, Netherlands) amplified a 1 kHz TTL trigger signal with a 30% duty cycle to create a 1 kHz square wave signal that oscillates between 0 and 25 V. The maximum bias voltage is adjustable. The 30% duty cycle for the bias ensured that the device returned to ambient temperature before the next biasing cycle began. The bias equipment's output aligned with the camera's 4 Hz trigger signal to alternate between the bias 'ON' and 'OFF' phases as depicted in figure 3. To image thermal transients continuously, the integrated driver module incrementally adjusted the time delay between the driving current signal and the bias equipment's output. The camera captured four I images during the bias 'ON' and 'OFF' periods. A time-resolved thermoreflectance signal ($\Delta R/R$) was derived by calculating the differences between images acquired during these ON/OFF periods. This process allowed for the analysis of thermal changes over time, providing insights into the transient thermal behavior of the sample.

Figure 2 illustrates the sample design used to validate the performance of the dual-mode TRM system. The sample consists of a thin-film polycrystalline silicon (poly-Si) resistor, 500 nm in thickness, equipped with Cr/Au ohmic contacts, each 50 and 200 nm in thickness, on a silicon dioxide (SiO_2) layer of thickness 500 nm, all mounted on a Si substrate with a thickness of 700 μm. The SiO_2 layer functions as a thermal insulator, designed to minimize heat dissipation into the Si substrate. The poly-Si microresistor features a bow-tie shape, with dimensions including a length of 100 μm, a width of 15 μm, and a central square size measuring 5 μm across. The resistance of the ohmic device was measured to be 9.3 kΩ. This design ensured that maximum heat generation occurred at the center, from where it spread towards both ends.

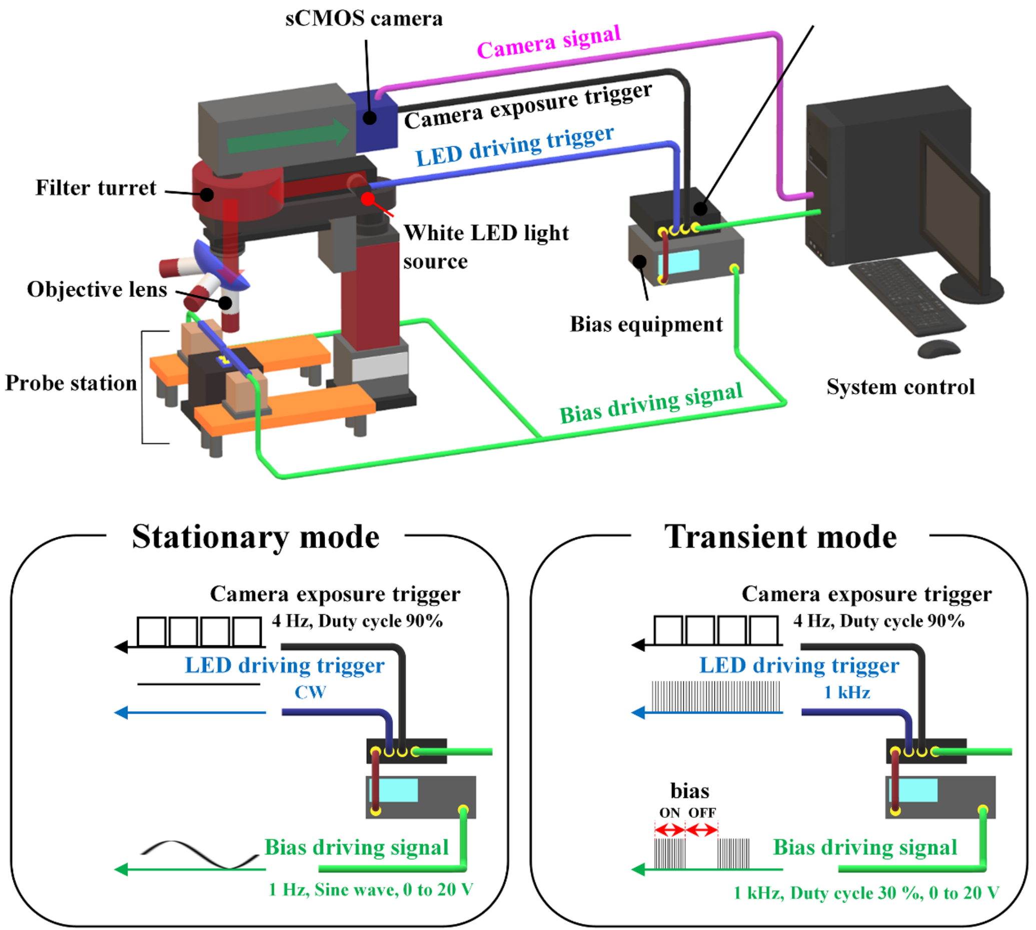

Figure 1. A schematic of the dual-mode TRM system and its imaging modes.

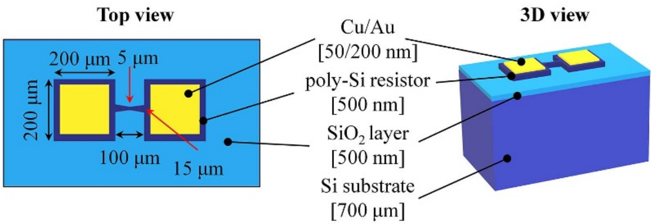

Figure 2. Schematic of a polysilicon (poly-Si) microresistor situated on SiO_2 layer atop silicon (Si) substrate.

3. Principle of TRM

TRM is based on measurement of changes in a sample's surface reflectivity relative to temperature variations. This relation can be approximated as equation (1) [3, 26]:

$$\frac{\Delta R}{R} \approx \frac{1}{R}\frac{\partial R}{\partial T}\Delta T = \kappa \Delta T \tag{1}$$

where R and T denote the reflectivity and temperature at the sample's surface, respectively. Here, ΔR represents the change in sample surface reflectivity because of a change in local surface temperature (ΔT), and κ represents the thermoreflectance coefficient. This coefficient can vary depending on intrinsic material properties, such as composition and sample structure, as well as microscopic configurations, including the illumination, wavelength, and numerical aperture of the objective lens [27, 28]. Given that the thermoreflectance coefficient for microelectronic devices typically ranges from 10^{-5} to 10^{-3} K^{-1}, the relative changes in reflectivity to be measured are small. Therefore, in the TRM for detecting subtle thermal changes, choosing an optimal illumination wavelength and employing image processing techniques to isolate $\Delta R/R$ are crucial for improving the SNR [13, 29].

4. Stationary and transient thermal imaging method

For stationary thermal imaging, the four-bucket method, a homodyne lock-in detection technique, was used to detect $\Delta R/R$ for steady-state thermal characterizations [3, 30]. This method involves modulating the sample's temperature by applying a sinusoidal bias driving signal. The camera's exposure is triggered at a frequency of 4 f, synchronized with the bias driving signal at frequency f, resulting in the acquisition of four images during each period T of the bias driving signal. The LED illumination source operates in the CW mode. The $\Delta R/R$ image is subsequently derived from the four collected images, labeled as I_1, I_2, I_3, and I_4, using

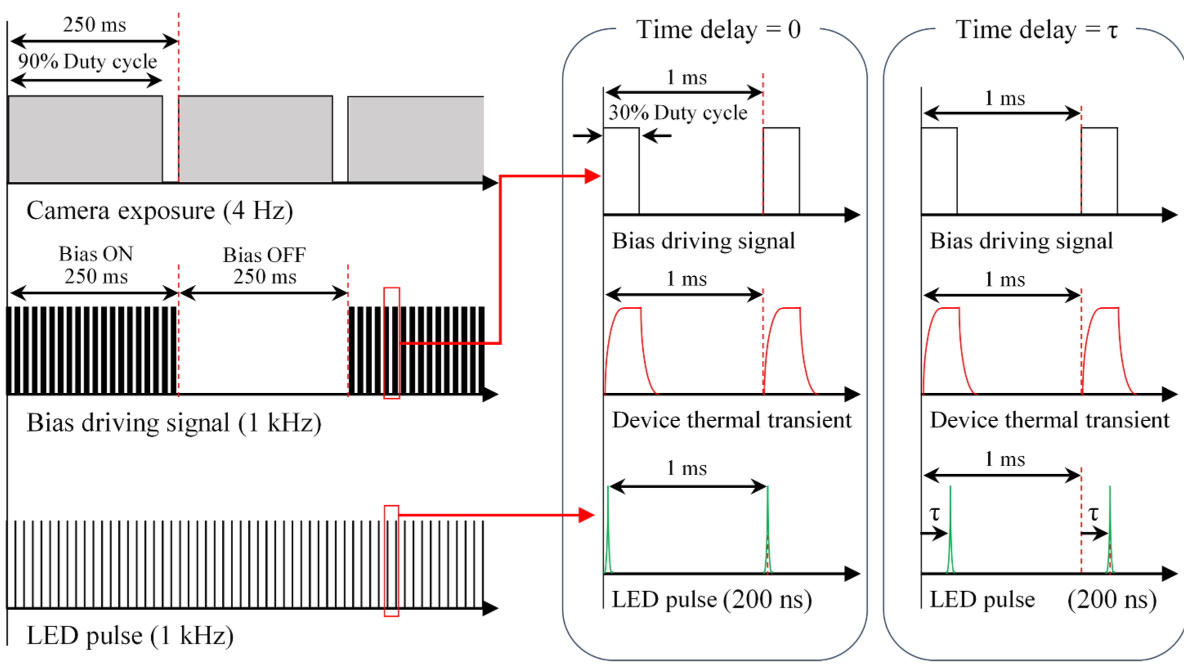

Figure 3. Timing diagram depicting the transient mode operation in the pulsed boxcar average method.

equation (2) [3, 31].

$$\frac{\Delta R(x,y)}{R(x,y)} = \frac{\pi}{\sqrt{2}} \frac{\sqrt{(I_1 - I_3)^2 + (I_2 - I_4)^2}}{I_1 + I_2 + I_3 + I_4}. \quad (2)$$

However, to capture $\Delta R/R$ images of thermal transients that occur faster than the camera's frame rate, the pulsed boxcar averaging method is implemented [18, 19]. This transient thermal imaging technique allows for the visualization of rapid transient phenomena by using pulsed device excitation along with pulsed illumination. Figure 3 includes a timing diagram that outlines the camera exposure time, bias application, and LED pulse duration, demonstrating the precise synchronization and timing delays of control signals in transient mode. This measure facilitates the sequential timing of time-dependent thermal responses. With the increase in temporal resolution, the illumination pulse duration decreased, resulting in a reduction in the amount of light that the camera can detect [32–34]. However, as depicted in figure 3, by accumulating multiple illumination pulses during the camera's exposure time, a satisfactory SNR can be achieved even with rapid thermal transients

$$\frac{\Delta R(x,y)}{R(x,y)} = \frac{R(x,y)_{\mathrm{ON}} - R(x,y)_{\mathrm{OFF}}}{R(x,y)_{\mathrm{OFF}}}. \quad (3)$$

Time-resolved $\Delta R/R$ images can be extracted from I images obtained during the 'ON' and 'OFF' bias phases at specific instances of illumination, referred to as time delay, as described in equation (3) [33]. Therefore, by repeatedly conducting this image analysis and adjusting the illumination's time delay with microsecond or sub-microsecond pulse widths, a series of thermal activities within the microsecond or sub-microsecond temporal range can be examined. Here, for the transient mode, synchronization between the LED pulse and the device thermal transient was conducted as followings. First, the time difference between the LED pulse monitoring signal provided by the driver module and optical detector output for the LED pulse illumination generated by the driving current signal was measured. Second, while watching both the LED pulse monitoring signal and bias equipment output for the applied bias voltage on the oscilloscope, the output timing of the driving current signal was controlled for synchronization between the LED pulse and device thermal transient. It was assumed that the LED pulse monitoring signal and driving current signal on the driver module was synchronized. The minimum control level of the output timing was up to 5 ns based on the internal reference clock divided by the digital clock manager.

5. Results and discussion

Selecting an illumination wavelength with a high thermoreflectance coefficient enables the acquisition of high SNR $\Delta R/R$ images by enhancing the system's thermal sensitivity. Therefore, the thermoreflectance spectrum, indicating the magnitude of $\Delta R/R$ across wavelength, is crucial for choosing the illumination wavelength. Studies have revealed that spectroscopic TRM systems can identify this optimal wavelength from the thermoreflectance spectrum measured at high spectral resolution (on the order of nanometers) using a diffraction grating and a charge-coupled device camera [21]. These systems incorporate a liquid crystal tunable BPF that enables flexible selection of both the central wavelength and the bandwidth of the transmission band, facilitating the

selection of the optimal illumination band from a broadband light source such as a halogen lamp. However, the combined configuration of spectroscopic and imaging optical systems in advanced spectroscopic TRM systems introduces complexity in both structure and configuration, reducing user accessibility. Conventional TRM systems are generally built by integrating a basic optical microscope with exchangeable single-color visible LEDs, which have a full width at half maximum (FWHM) ranging between 10 and 20 nm. These systems obtain $\Delta R/R$ images by selecting an appropriate illumination source. However, the choice of illumination wavelength is limited by the spectral range of the LED sources integrated into the microscope. In our study, we used an optical microscopy technique that combines a white LED source with a filter turret containing several BPFs. These BPFs allow selective transmission of specific wavelength bands from the white LED source, thereby addressing the limitations of optimizing illumination wavelengths with single-color visible LEDs. Consequently, the thermoreflectance spectrum can be measured with a spectral resolution defined by the FWHM of the BPF (e.g. 10 nm), enabling the selection of an optimal illumination wavelength. However, the spectral accuracy is dependent on the number of BPFs used.

A poly–Si microresistor, as depicted in figure 2, was used to evaluate the thermal imaging capabilities of the dual-mode TRM system. The thermoreflectance spectrum was derived from $\Delta R/R$ measurements at each wavelength (or BPF), obtained through $\Delta R/R$ images captured while sequentially switching the BPFs within the filter turret. The turret contains a removable module that can hold up to six filters. By sequentially replacing three interchangeable modules with 18 BPFs, passbands ranging from 460 to 630 nm could be selected at 10 nm increments. The BPFs exhibited an FWHM of 10 nm, which aligns with the characteristics of single-color visible LEDs. Figure 4(a) presents the thermoreflectance spectrum of the poly-Si microresistor, measured using a white LED source in conjunction with a filter turret. The spectral range is determined by the number of BPFs used. The spectrum data point was calculated by averaging and subsequently normalizing the $\Delta R/R$ values corresponding to the region of interest (ROI) in the $\Delta R/R$ image acquired through a specific BPF. The ROI was within the poly-Si area, as indicated in figure 4(e). The thermoreflectance spectrum peaked at 550 nm and was lowest at 490 nm. Therefore, the ideal illumination wavelength for the SUT was determined to be a BPF centered at 550 nm.

To showcase the stationary mode, intensity (I) images and stationary $\Delta R/R$ images were acquired as presented in figures 4(b)–(g), respectively. BPFs with central wavelengths of 510, 550, and 580 nm were used to investigate the variances in thermal sensitivity based on the illumination wavelength. In the I images, the poly-Si microresistor's shape remained clearly discernible across all illumination conditions. By contrast, the stationary $\Delta R/R$ images revealed the poly-Si microresistors only under optimal illumination conditions, which exhibited a high thermoreflectance coefficient. Furthermore, a notable increase in heat was observed in the central region of the SUT. This phenomenon can be attributed to its bowtie shape. The resistance of poly-Si escalates toward the center, resulting in considerable heat generation in the middle because of Joule heating. By comparing the SNR of each $\Delta R/R$ image, an enhancement in thermal sensitivity through the selection of the optimal illumination wavelength was verified.

The ratio of the mean $\Delta R/R$ in the ROI to the standard deviation of the adjacent background noise was recorded to be 8.64, 12.12, and 0.22, respectively. Therefore, even though the optimal illumination wavelength was selected from the thermoreflectance spectrum acquired with a low wavelength resolution of 10 nm, the imaging of minute heat propagation was feasible because of its elevated thermal sensitivity.

To demonstrate the transient mode for the same poly-Si micro resistor, the Joule heating effect was monitored from 0 to 3 μs with a temporal resolution of 200 ns following the biasing in the ON/OFF phase. Identical to the stationary mode, optimal illumination with a central wavelength of 550 nm and a FWHM of 10 nm was used but in a pulsed mode. Figure 5(a) displays a time-resolved $\Delta R/R$ image obtained from 0 to 2 μs, where thermal transients are apparent throughout the entire measurement timeframe. Joule heating became visible at the center of the SUT within 200 ns post-bias application. Figure 5(b) depicts the transient thermal behavior around the bowtie region of the device, as marked by the ROI in figure 5(a). The normalized $\Delta R/R$ values were derived by averaging and subsequently normalizing the $\Delta R/R$ from the ROI of each time-resolved $\Delta R/R$ image. The transient $\Delta R/R$ imaging results indicate that observing the device's Joule-heating effect during heating is feasible. The temporal resolution is determined by the pulse width of the illumination light source [35, 36]. As indicated in figure 5(c), the white LED light source was operated in a pulsed mode with an approximate pulse width of 200 ns. The pulse width of illumination from the objective lens was measured using a photodetector (DET10A2, Thorlabs, USA) with a rise time of 1 ns. The delay time of the LED driving current was adjusted to synchronize the initiation of both the bias application and LED driving current. Subsequent measurements were obtained at 200 ns intervals starting from the bias application time with a pulsed illumination of 200 ns. To mitigate the reduced SNR caused by the pulsed illumination, 400 frames for both the bias 'ON' and 'OFF' states were captured (with an acquisition time of 200 s) and subsequently averaged. Time-resolved $\Delta R/R$ images were produced in accordance with equation (3).

Figure 6 presents the comparison of thermal images between the stationary TRM and IRT systems for a poly-Si microresistor with a bow-tie shape, featuring dimensions of 200 μm in length, 30 μm in width, and a central square size of 10 μm across. The resistance of the ohmic device was measured to be 14.3 kΩ. This sample was selected due to the lower spatial resolution of IRT. The IRT system is composed of an infrared camera (FLIR SC5000, FLIR Systems, Inc.) equipped with an InSb detector and a 5$\times$ close-up lens (FLIR Systems, Inc.), allowing it to detect and utilize mid-infrared wavelengths in the range of 3–5 μm. Accurate

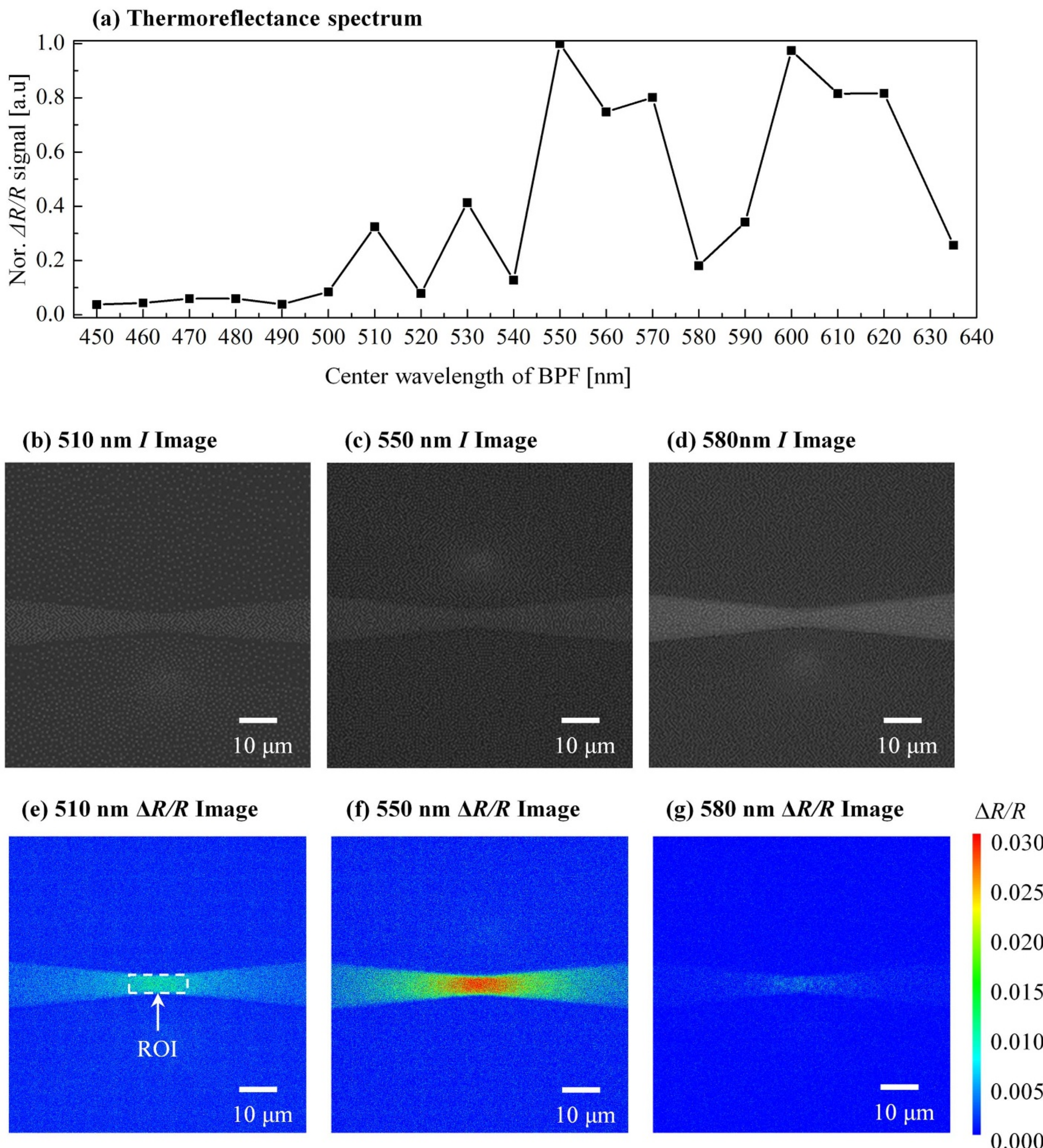

Figure 4. (a) Thermoreflectance spectrum with the *ΔR/R* signals normalized according to the wavelength of the incident illumination. (b)–(d) Intensity (*I*) images, and (e)–(g) stationary *ΔR/R* images. The *I* images of the poly-Si microresistor were captured at incident wavelengths of 510, 550, and 580 nm, using a 50× objective lens.

temperature measurements of the IRT system were carried out as described in our previous work [12]. The T image of the stationary TRM was calculated using the thermoreflectance coefficient (κ) and equation (1). The coefficient κ for poly-Si was determined to be 7.82×10^{-4} K^{-1}, with an optimal wavelength of 550 nm, following typical procedures in TRM [21, 34]. From equation (1), the determination of the thermoreflectance coefficient κ can be performed by measuring the relative reflectivity variation as a function of the temperature variation. The temperature variation measurement of the sample was conducted by a Peltier element and a resistive temperature detector using a feedback temperature controller (2510-AT, KEITHLEY, USA). During the temperature variation, the reflectivity measurement for the sample was repeated at each set temperature using the reflection image acquired by the experimental set-up. A linear relation between the relative reflectivity and temperature variations were recorded and the slop (κ) was calculated via linear fitting. As shown in figure 6, thermal images of the poly-Si microresistor were captured using both the stationary TRM and IRT systems under a constant bias voltage of 30 V, with the background temperature maintained at 25 °C. The average temperatures

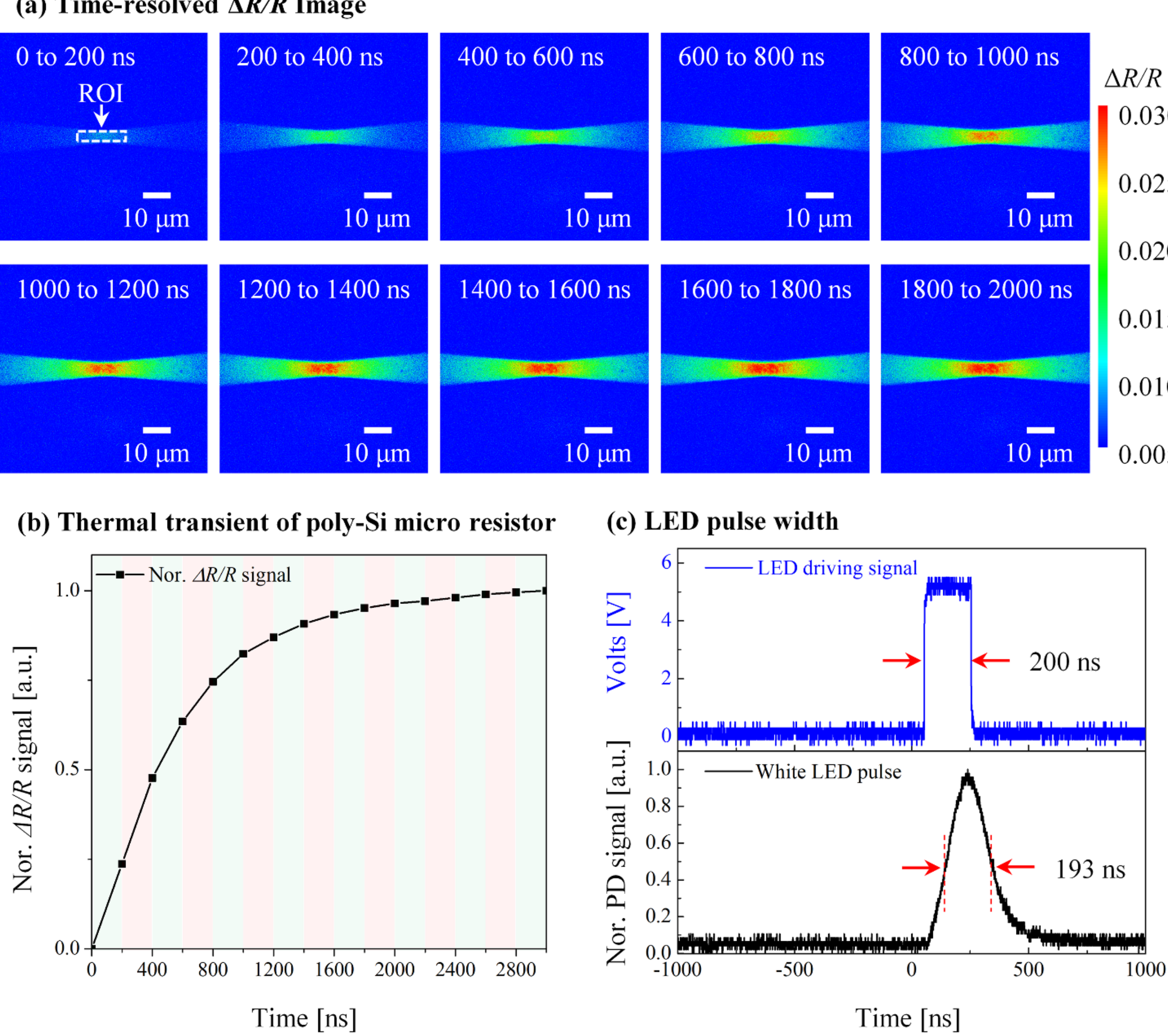

Figure 5. (a) Time-resolved $\Delta R/R$ image from 0 to 2000 ns with 200 ns temporal resolution, (b) thermal transient in a poly-Si microresistor caused by Joule heating, and (c) the pulse width of white LED source corresponding to an LED driving signal of 200 ns.

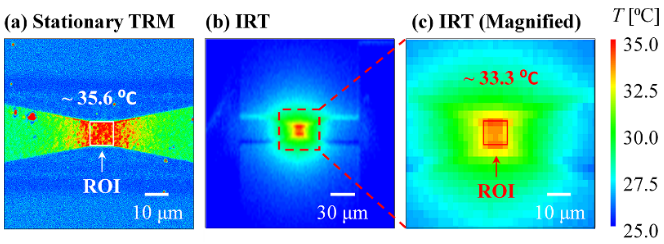

Figure 6. Temperature images of a polysilicon micro-resistor measured by the (a) stationary TRM and (b) IRT system at bias voltages of 30 V, and (c) a magnified temperature image of the region marked with dotted line in (b) from the IRT system.

measured in the ROI marked in the images were approximately 33.3 °C for stationary TRM and 35.6 °C for IRT, respectively. Although there was a minor difference between the two measurements, this comparison serves to validate the reliability of the TRM system, as the results from the TRM closely agree with those from the well-established IRT method. In addition, the TRM system offers a much sharper thermal distribution image compared to the IRT system, owing to its superior spatial resolution.

Figures 7(a) and (b) present the temperature change (ΔT) images of the poly-Si microresistor, acquired from $\Delta R/R$ images in both stationary and transient modes at an identical bias level of 20 V. The ΔT images were calculated using the thermoreflectance coefficient (κ) and equation (1). To assess the reliability of thermal distribution across both modes, the ΔT image from the stationary mode was compared with the time-resolved ΔT image obtained under thermal steady-state conditions in the transient mode, which was captured at 10 000 ns after bias application. Figure 7(c) shows the line profiles (A, B) across the maximum heat generation area in each mode, averaged over ten rows near the A and B lines in figures 7(a) and 6(b), respectively. Despite some noise differences in line profiles (A, B), the profiles exhibited the same overall trend, indicating a consistent central region

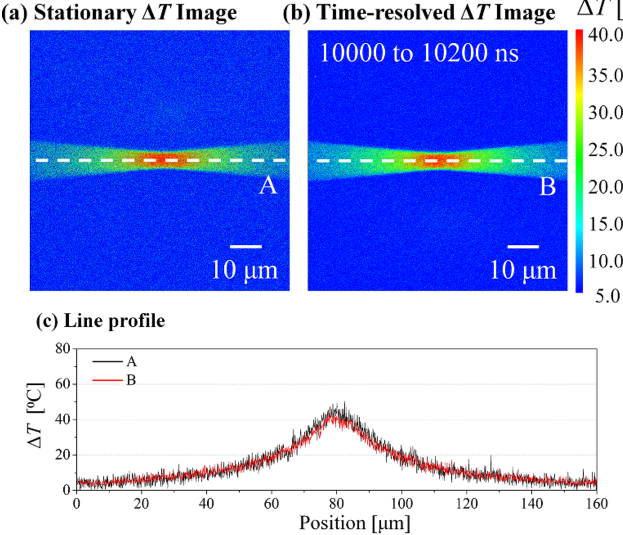

Figure 7. (a) Stationary temperature change (ΔT) image at a bias level of 20 V in stationary mode, (b) time-resolved ΔT image under the thermal steady-state condition at 20 V in the transient mode, and (c) line profile across the maximum heat generation area in each mode.

temperature of approximately 40 °C in the SUT across both modes.

6. Conclusion

This study introduced a highly sensitive dual-mode TRM system for analyzing both the stationary and transient thermal characteristics of microelectronic devices. The primary advantage of our system is that it allows for thermal imaging with optimal illumination. A simple system configuration based on standard optical microscopy was devised. The optimal illumination, which provides high thermal sensitivity for the SUT, was determined based on the thermoreflectance spectrum obtained using a white LED light source and a filter turret. The system's performance in imaging thermal phenomena, both in stationary and transient modes, was demonstrated using the four-bucket and pulsed boxcar averaging methods, respectively. This demonstration revealed that the enhanced thermal sensitivity, achieved through optimal illumination, enabled the observation of distinct thermal distributions and the monitoring of thermal propagation with high temporal resolution. The system exhibits considerable potential for using an analytical tool with sub-micron resolution in the spatiotemporal domain to evaluate the heat generation behavior of microelectronic devices. Analyzing the stationary thermal distribution and transient thermal transfer within these devices can provide insights into their physical mechanisms and limitations associated with self-heating.

Data availability statement

All data that support the findings of this study are included within the article (and any supplementary files).

Acknowledgments

This research was supported by the Korea Basic Science Institute (Grant No. B437600), the National Research Foundation of Korea (Grant No. 2021M3H4A6A03103722), and the National Research Council of Science & Technology (NST) grant by the Korean government (MSIT) (No. GTL24041-000).

ORCID iDs

Chan Bae Jeong https://orcid.org/0000-0002-7892-8410
Dong Uk Kim https://orcid.org/0000-0002-6124-9251
Ilkyu Han https://orcid.org/0000-0002-5434-3039
Dongmok Kim https://orcid.org/0000-0002-5291-9110
Hwan Hur https://orcid.org/0000-0002-0854-9693
I Jong Kim https://orcid.org/0000-0001-8158-8042
Kye-Sung Lee https://orcid.org/0000-0001-8669-627X
Jung-Dae Kim https://orcid.org/0000-0001-7939-2278
Woo June Choi https://orcid.org/0000-0003-0793-2735
Ki Soo Chang https://orcid.org/0000-0002-6067-2066

References

[1] Kölzer J, Oesterschulze E and Deboy G 1996 *Microelectron. Eng.* **31** 251–70
[2] Liu W and Yang B 2007 *Sens. Rev.* **27** 298–309
[3] Farzaneh M, Maize K, Lu¨erßen D, Summers J A, Mayer P M, Raad P E, Pipe K P, Shakouri A, Ram R J and Hudgings J A 2009 *J. Phys. D: Appl. Phys.* **42** 143001–21
[4] Garimella S V *et al* 2008 *IEEE Trans. Compon. Packag. Technol.* **31** 801–15
[5] Joshi Y K and Garimella S V 2003 *Microelectron. J.* **34** 169
[6] Ziabari A *et al* 2018 *Nat. Commun.* **9** 255
[7] Vermeersch B, Mohammed A M S, Pernot G, Koh Y R and Shakouri A 2015 *Phys. Rev.* B **91** 085203
[8] Crépel O, Beaudoin F, De Morais L D, Haller G, Perdu P, Desplats R and Lewis D 2002 *Microelectron. Reliab.* **42** 1741–6
[9] Barton D L and Tangyunyong P 1996 *Microelectron. Eng.* **31** 271–9
[10] Liu Z, Feng Y, Li H, Cao N and Qiu L 2024 *Int. J. Heat Mass Transf.* **232** 125979
[11] Gordiyenko E, Fomenko Y, Shustakova G, Kovalov G and Shevchenko S 2024 *Rev. Sci. Instrum.* **95** 035116
[12] Chang K S, Yang S C, Kim J Y, Kook M H, Ryu S Y, Choi H Y and Kim G H 2012 *Sensors* **12** 4648–60
[13] Mayer P M, Lu¨erßen D, Ram R J and Hudgings J A 2007 *J. Opt. Soc. Am.* **24** 1156
[14] Kim D U, Kim J D, Han I, Jeong C B, Lee K-S, Hur H, Nam K-H, Bae J Y, Kim I J and Chang K S 2020 *IEEE Trans. Instrum. Meas.* **69** 2914–23
[15] Kim D U, Jeong C B, Kim J D, Lee K S, Hur H, Nam K H, Kim G H and Chang K S 2017 *Sensors* **17** 2774
[16] Kendig D, Yazawa K, Marconnet A, Asheghi M and Shakouri A 2012 *28th IEEE Semi-Therm Symp. (San Jose, CA, USA)* pp 344–7
[17] Ryu S Y, Kim D U, Kim J K, Choi H Y, Kim G H and Chang K S 2014 *Int. J. Thermophys.* **36** 1217–25
[18] Vermeersch B, Christofferson K J, Maize K, Shakouri A and De Mey G 2010 *26th IEEE Semi-Therm Symp. Santa Clara CA USA* pp 228–34
[19] Maize K and Shakouri A 2008 *24th IEEE Semi-Therm Symp. (San Jose, CA, USA)* pp 55–58

[20] Bahk J H and Shakouri A 2019 *2019 IEEE BCICTS Symp. (Nashville, TN, USA) pp 1–7*, DOI: (https://doi.org/10.1109/BCI-CTS45179.2019.8972732)
[21] Kim D U, Park K S, Jeong C B, Kim G H and Chang K S 2016 *Opt. Express* **24** 13906–16
[22] Heller J, Bartha J W, Poon C C and Tam A C 1999 *Appl. Phys. Lett.* **75** 43–45
[23] de Freitas L R, da Silva E C, Mansanares A M, Tessier G and Fournier D 2005 *J. Appl. Phys.* **98** 063508
[24] Tessier G, Hole´ S and Fournier D 2001 *Appl. Phys. Lett.* **78** 2267–9
[25] Tessier G, Jerosolimski G, Hole S, Fournier D and Filloy C 2003 *Rev. Sci. Instrum.* **74** 495–9
[26] Lu¨erßen D, Hudgings J, Mayer P and Ram R 2005 *21th IEEE Semi-Therm Symp. (San Jose, CA, USA)* pp 253–8
[27] Favaloro T, Bahk J H and Shakouri A 2015 *Rev. Sci. Instrum.* **86** 024903
[28] Alajlouni S and Shakouri A 2022 *Rev. Sci. Instrum.* **93** 103701
[29] Choi W J, Ryu S Y, Kim J K, Kim D U, Kim G H and Chang K S 2013 *Opt. Lett.* **38** 3581–4
[30] Braun J L, Olson D H, Gaskins J T and Hopkins P E 2019 *Rev. Sci. Instrum.* **90** 024905
[31] Grauby S, Forget B C, Hole´ S and Fournier D 1999 *Rev. Sci. Instrum.* **70** 3603–8
[32] Becher N, Farzaneh M, Knipfer B, Sigler C, Kirch J, Boyle C, Botez D, Mawst L J, Lindberg D F III and Earles T 2019 *J. Appl. Phys.* **125** 033102
[33] Garcia V G and Farzaneh M 2016 *J. Appl. Phys.* **119** 045105
[34] Tessier G, Polignano M-L, Pavageau S, Filloy C, Fournier D, Cerutti F and Mica I 2006 *J. Phys. D: Appl. Phys.* **39** 4159–66
[35] Kerry M 2014 *High Resolution Thermoreflectance Imaging of Power Transistors and Nanoscale Percolation Networks* (University of California)
[36] Vermeersch B, Bahk J H, Christofferson J and Shakouri A 2013 *J. Appl. Phys.* **113** 104502